Available online at www.sciencedirect.com
SCIENCE DIRECT
Polymer 46 (2005) 1181–1188
polymer
www.elsevier.com/locate/polymer

Synthesis of cationic poly(methyl methacrylate)-poly(*N*-isopropyl acrylamide) core-shell latexes via two-stage emulsion copolymerization

Andrea M. Santos[a], Abdelhamid Elaïssari[b], José M.G. Martinho[a], Christian Pichot[b,*]

[a]*Centro de Química-Física Molecular, Instituto Superior Técnico, Av. Rovisco Pais, 1, 1049-001 Lisboa, Portugal*
[b]*Unité Mixte CNRS-bioMérieux, UMR-2714, ENS Lyon, 46 allée d'Italie, 69364 Lyon Cedex 07, France*

Accepted 30 September 2004
Available online 8 December 2004

Abstract

Thermally sensitive poly(methyl methacrylate (MMA))-poly(*N*-isopropylacrylamide (NIPAM)) core-shell particles were prepared via a two-stage emulsion copolymerization process. Methylene bisacrylamide (MBA), 2,2′-azobis (2-amidinopropane) dihydrochloride (V50) and dodecylethyl dimethyl ammonium bromide (DEDAB) were used as crosslinker, cationic initiator and surfactant, respectively. Functional core-shell particles were prepared using aminoethyl methacrylate hydrochloride (AEMH) as cationic co-monomer to increase the surface charge density. The influences of the crosslinker and co-monomer concentrations on the thickness and swelling capacity of the PNIPAM-based shell layer were studied. The latex particle size and particle size distribution were determined both by dynamic light scattering (DLS) and scanning electron microscopy (SEM). Monodisperse particles were produced with diameters between 150–250 nm (at 25 °C) and 140–190 nm (at 50 °C). The surface charge density was determined by chemical titration and higher values (~10 μmol/g) were obtained for the functional core-shell particles. The electrokinetic properties of the dispersions at several pH and temperature values confirm the presence of the shell layer and cationic surface charges.

Keywords: Thermal sensitive core-shell particles; Functional cationic groups; Two-stage emulsion copolymerization

1. Introduction

Core-shell particles with hydrophobic cores and thermo-sensitive shells are very useful in biomedical applications, such as vectors for drug delivery or in the purification of proteins and DNA [1–4]. The thermo sensitivity is mainly due to the properties of poly(*N*-alkylacrylamide) or poly(*N*-alkylmethacrylamide) polymers that usually form the particle shell. Among these polymers, poly(*N*-isopropyl acrylamide) (PNIPAM), has been the most studied mainly because its lower critical solution temperature (LCST) occurs at 32 °C, that is close to the physiologic temperature [5]. Core-shell particles bearing a PNIPAM shell show a volume phase transition (VPT) upon heating above the LCST of the PNIPAM in aqueous solution. The shrink of the shell above the volume phase transition temperature (T_{VPT}) occurs owing to the release of the water entrapped in the shell induced by attractive segmental interactions between the hydrophobic isopropyl groups of the PNIPAM chains.

The first synthesis of this kind of materials was performed by Makino et al. [6] and Zhu et al. [7], that prepared poly(styrene)-poly(*N*-isopropylacrylamide) (PS-PNIPAM) core-shell particles by a two-stage emulsion copolymerization process. Later on, Duracher et al. [8] synthesized PS-PNIPAM core-shell particles containing the functional monomer, aminoethyl methacrylate hydrochloride (AEMH), using both batch and shot-growth polymerization processes. Recently, Xiao et al. [9] synthesized poly(acrylamide-*co*-styrene)-poly(acrylamide-acrylic acid) particles whose shell swells by temperature increase. The thermal behavior of these particles is opposite to the one of those bearing a PNIPAM shell, which opens the opportunity for new applications.

This work describes the synthesis of thermal sensitive PMMA-PNIPAM core-shell nanoparticles by a two-stage emulsion copolymerization process. These particles should

* Corresponding author. Tel.: +33 72 72 81 00; fax: +33 4 72 72 85 33.
E-mail address: christian.pichot@ens-lyon.fr (C. Pichot).

0032-3861/$ - see front matter © 2004 Elsevier Ltd. All rights reserved.
doi:10.1016/j.polymer.2004.11.069

be used as supports for proteins and oligonucleotides that will be probed by fluorescence. For this purpose, the colloidal particles should fulfill the following requirements: (i) being transparent in the region of absorption of the protein intrinsic fluorophores (tyrosine; tryptophan); (ii) being of small size (~200 nm) and monodisperse to avoid the spurious scattered light. The latex particles were characterized in terms of size and polydispersity by scanning electron microscopy (SEM) and dynamic light scattering (DLS), while the charge and charge distribution were estimated from the zeta potential and chemical titration, at several pH and temperature values.

2. Experimental part

2.1. Materials

Methyl methacrylate (MMA, from Aldrich, 99%) was distillated in vacuum before use. *N*-isopropylacrylamide (NIPAM, from Acros, 99%) was recrystallized in a toluene/pentane mixture (60/40; v/v) before use. The 2,2′-azobis(2-amidinopropane) dihydrochloride (V50, from Wako Chemicals) was purified by recrystallization from a water/acetone mixture. *N*-(3-aminopropyl) methacrylamide hydrochloride (APMH, from Polysciences), aminoethyl methacrylate hydrochloride (AEMH, from Acros, 99%), methylene bisacrylamide (MBA, from Kodak, electrophoresis grade), dodecylethyl dimethyl ammonium bromide (DEDAB, from Fluka AG, >98%), sodium hydrogen carbonate (from Merck, p.a.) and sodium dodecyl sulfate (SDS, from Fluka Chemika, p.a.) were used as received.

Sodium hydrogencarbonate (from Aldrich, ACS reagent), sodium carbonate (from Aldrich, ACS reagent), 4-dimethyl aminopyridin (DMAP; from Aldrich, 99%), dithiothreitol (DTT; from Aldrich, 99%), 1,4-dioxan (RH, Spectranal) and *N*-succinimidyl-3-(2-pyridyldithio) propionate (SPDP, from Pierce) were used as received. Deionized water from Millipore was boiled under nitrogen and was used in all polymerizations.

2.2. Synthesis of the latexes

2.2.1. Preliminary batch polymerizations

PMMA particles bearing positive surface charges were synthesized by batch emulsion polymerization using the recipes shown in Table 1 for 60 g H_2O and 5 g MMA. A reactor of 50 ml equipped with a glass anchor-type stirrer running at 300 rpm, condenser and nitrogen inlet and outlet was used. Several runs were performed at constant temperature (70 °C) in the absence of surfactant using V50 as initiator and two functional co-monomers, APMH and AEMH. Some latexes were also prepared using several amounts of surfactant, DEDAB, in the absence of functional co-monomers.

2.2.2. Two-stage copolymerization

Two sets of core-shell latexes (*cssgp1–4* and *cssgpf1–4*) were prepared by a two-stage emulsion copolymerization process using DEDAB as surfactant. In a common stage, a batch polymerization was performed using MMA/DEDAB/V50 until 70–80% polymerization conversions. In a second stage, a mixture of NIPAM/MBA or NIPAM/MBA/AEMH was added in several shots to the reaction medium. The recipes are shown in Table 2 for 60 g H_2O (*cssgp1–4*), 65 g H_2O (*cssgpf1–4*), 0.05 g V50, 0.06 g/100 g DEDAB and 5 g MMA.

The polymerizations were performed at 70 °C for at least 2 h in a 50 ml reactor. The *cssgp* set was prepared using several amounts of crosslinker while for the *cssgpf* series the amount of crosslinker was fixed, being varied the concentration of the AEMH co-monomer.

2.2.3. Polymerization kinetics

Instantaneous and global polymerization conversions were determined by gravimetry. The solid content at a given polymerization time, SC (t), was determined and the percentage conversion, %C(t), calculated by,

$$\%C(t) = \frac{\mathrm{SC}(t)}{\mathrm{SC}(\infty)} \times 100 \quad (1)$$

where SC(∞) is the solid content for a complete polymerization reaction.

2.3. Colloidal characterization

The latex particles were cleaned by repetitive centrifugation and redispersion cycles using Milli-Q water before the electrokinetic and swelling experiments.

2.3.1. Particle size and size distribution

Scanning electron microscopy (SEM) micrographs of the latexes were obtained with a Hitachi (model S 2400) microscope. The samples were prepared by placing a drop of a highly diluted dispersion in a coal sample holder, and let dry before being sputtered with gold. From the images, the particles shape was deduced.

The hydrodynamic particle size and size distribution of the latexes were determined by dynamic light scattering (DLS) using a Zetasizer from Malvern Instruments (model 3000-HS). The diameters of highly diluted dispersions (in 10^{-3} M HCl) were measured, at several temperatures between 20 and 50 °C. Each data point was the average of at least three measurements.

2.3.2. Electrokinetics

The electrophoretic mobility (μ_e) of the latex particles was measured at several pH (25 °C) and temperatures (10^{-3} M HCl; pH ~ 3) using the ZetaSizer from Malvern Instruments (3000-HS model). The zeta potential (ζ) was calculated from the electrophoretic mobility using the Smoluchowski's

Table 1
Preliminary batch emulsion copolymerization recipes

Latex	m_{APMH} (g)	m_{AEMH} (g)	m_{V50} (g)	m_{DEDAB} (g/100 g)
pmma+1	0	0	0.051	0
pmma+2	0.050	0	0.052	0
pmma+3	0.15	0	0.051	0
pmma+4	0.25	0	0.050	0
pmma+5	0	0.051	0.051	0
pmma+6	0	0.051	0.10	0
pmma+7	0	0.10	0.051	0
pmma+8	0	0	0.051	0.0050
pmma+9	0	0	0.050	0.029
pmma+10	0	0	0.051	0.061

equation,

$$\varsigma = \frac{\eta}{\varepsilon}\mu_e \tag{2}$$

where η is the viscosity and ε the permittivity of the medium [10].

2.3.3. Surface charge density

The available amount of amine and amidine groups on the latex surface was determined by a slightly modified procedure reported elsewhere [11]. The titration was performed by adding to 500 μl of washed latex samples (5% wt/v), 500 μl of a carbonate/bicarbonate buffer solution (50 mM; pH = 9.2) and 5 μL of SPDP (0.5 M in dioxan) in the presence of a catalyst (DMAP). The mixture was stirred for ~100 min at room temperature and centrifuged afterwards (15,000 rpm; 20 min). The supernatant was removed to a vial (wash 1) and the particles were resuspended in 1 ml of the carbonate/bicarbonate buffer solution. The centrifugation/resuspension step was repeated and the supernatant was collected (wash 2). Reduction of the disulfide bonds was performed by adding 50 μl of a DTT solution (50 mM) to the samples. After ~30 min of incubation at room temperature, the samples were centrifuged and the supernatants were collected. The optical densities (OD) at 343 nm and 20 °C were determined using a UV/Vis absorption spectrometer (JASCO V-560). All samples were diluted 20 times before the OD measurements and the values are averages of three measurements.

The SPDP coupling yield, Y was calculated from Eq. (3) where OD_L, OD_1 and OD_2 are the optical densities of the latex and wash 1 and 2 supernatants, respectively.

$$Y = \frac{OD_L}{OD_L + OD_1 + OD_2} \tag{3}$$

The overall latex surface charge, σ (μmol/g of latex) was then calculated from Eq. (4), where C_i is the initial SPDP quantity (2.5 μmol) and P the amount of latex particles (0.025 g).

$$\sigma = \frac{Y \times C_i}{P} \tag{4}$$

Table 2
Two-stage emulsion copolymerization recipes

Latex	m_{AEMH} (g)	m_{NIPAM} (g)	m_{MBA} (g)
cssgp1	0	0.92	0.00
cssgp2	0	0.90	0.05
cssgp3	0	0.89	0.10
cssgp4	0	0.91	0.15
cssgpf1	0.014	0.90	0.10
cssgpf2	0.031	0.88	0.10
cssgpf3	0.046	0.90	0.10
Cssgpf4	0.014	1.79	0.10

3. Results and discussion

3.1. Preliminary batch polymerizations

Several polymerization runs were performed in order to obtain monodisperse positively charged PMMA cores with diameter around 100 nm using V50 as initiator and adding the surfactant DEDAB or functional co-monomers APMH and AEMH. The recipes in Table 1 were adapted from those used in the synthesis of negatively charged PMMA latexes [12]. Table 3 shows the hydrodynamic particle diameter (D_p), particles number (N_p), overall conversions (%C) and percentage of water-soluble polymers (%wsp).

The number of particles was estimated by Eq. (5),

$$N_p \approx \frac{m}{\rho \frac{4}{3}\pi R_p^3} \tag{5}$$

where, ρ is the density of PMMA at 20 °C (1.19 g cm^{-3}), m is the mass of particles and R_p their hydrodynamic radius [13].

For all batch polymerization runs, the final conversions were higher than 70% after 30 min of reaction. Without adding the functional monomer or surfactant to the batch polymerization recipe (run *pmma+1*), particles with diameters around 350 nm were obtained. In order to reduce the particle size, functional monomers (APMH, AEMH) and a cationic surfactant (DEDAB) were used. When functional monomer was added, particles with diameters between 300

Table 3
Hydrodynamic particle diameter (D_p), particle number (N_p), overall conversions (%C) and water-soluble polymers (%wsp) for the cationic PMMA latexes

Latex	D_p (nm)	$N_p/10^{14}$ (L^{-1})	%C	%wsp
pmma+1	350	–	70–75	1.20
pmma+2	338	3.1	97	1.63
pmma+3	Non-stable			
pmma+4	Non-stable			
pmma+5	284	5.2	96	1.45
pmma+6	328	3.3	93	2.80
pmma+7	383	2.1	97	1.80
pmma+8	279	5.5	97	0
pmma+9	174	22.8	98	0.60
pmma+10	134	49.7	97	1.56

and 400 nm were found (runs *pmma+2–pmma+7*). By increasing the APMH concentration unstable dispersions were obtained, probably due to the high formation of water-soluble polymers. When using AEMH, the increase of the initiator and functional monomer concentrations led to the formation of polydisperse latex dispersions with a high content of water-soluble polymers. By addition of a cationic surfactant (DEDAB) at concentrations below its CMC ($CMC_{DEDAB} \sim 4.56$ g/l, determined by conductimetry) smaller and monodisperse particles were obtained. The increase of the DEDAB concentration (runs *pmma+8–10*), raises the initial polymerization rate, reduces the nucleation period and increases the particle number (N_p). At 1/8 CMC_{DEDAB} (run *pmma+10*), latex particles with diameters around 130 nm were finally obtained.

3.2. Two-stage copolymerizations

A two-stage emulsion copolymerization process was used to produce cationically-charged PMMA/PNIPAM core-shell latexes. Initially, a batch polymerization similar to the one optimized before, was allowed to run until the MMA conversion is around 70–80%. The diameters of the particles at the end of this stage were around 130 nm. Then, a mixture containing NIPAM/MBA or NIPAM/MBA/AEMH was added in several shots to better control the formation of the PNIPAM shell around the PMMA core. The shots were performed at high MMA conversions to favor the formation of monodisperse particles with smoother shells covering the entire PMMA core. Besides this, the addition of NIPAM under starved conditions avoids the formation of PNIPAM particles [14].

For the polymerization runs (*cssgp1–4*), no functional monomer was added and the crosslinker (MBA) concentration was varied from 1 to 3% wt/wt MBA/MMA. Irrespective of the MBA concentration, the conversion was ~100% and the percentage of water-soluble polymers was of the order of 2% wt.

The final polymerization runs (*cssgpf 1–4*) were performed with an MBA content ~1% wt/wt and several AEMH concentrations ~0.3–0.9% wt/wt AEMH/MMA. In the last polymerization run (*cssgpf4*) the NIPAM content was increased by two times in an attempt to obtain latex particles with thicker shell layers. The global conversions were ~100%, and the water-soluble polymer contents varied from 3 to 6% wt with the amount of AEMH. The amount of water-soluble polymer increased probably due to: (i) a copolymerization effect based on the three times increase in the reactivity ratio of methacrylate when compared to that of acrylamide [15]; (ii) a chain transfer reaction between AEMH and NIPAM that leads to a decrease of the molecular weight of the PNIPAM chains [8].

3.3. Core-shell latex characterization

The PMMA-PNIPAM core-shell latexes were characterized in terms of particle size, size distribution, electrokinetic behaviour and surface charge density. Fig. 1 shows the SEM pictures of the *pmma+10*, *cssgp3* and *cssgpf3* core-shell latex dispersions. The particles are almost spherical and monodisperse. This is a consequence of the following: (i) the nucleation step is faster than the particle growth in the batch stage; (ii) the aggregation of particles does not occur during its growing due to their surface charge density (coming from the initiator, V50) and to the additional stabilization imparted by the DEDAB; (iii) the shot growth was carried out after the monomer conversion in the seed is higher than 70%, which avoids a secondary nucleation.

3.3.1. Particle size and size distribution

The particle diameters of the latexes (D_p) were determined by DLS at 25 and 50 °C. The hydrodynamic shell thickness increment (δ_{shell}) and swelling factor (SF) were determined from the hydrodynamic diameters by Eqs. 6 and 7.

$$\delta_{shell} = \frac{(D_p^{25^\circ} - D_p^{50^\circ})}{2} \quad (6)$$

$$SF = \left(\frac{D_p^{25^\circ}}{D_p^{50^\circ}}\right)^3 \quad (7)$$

Table 4 shows the values calculated at several temperatures. The particle hydrodynamic diameters at 50 °C are smaller

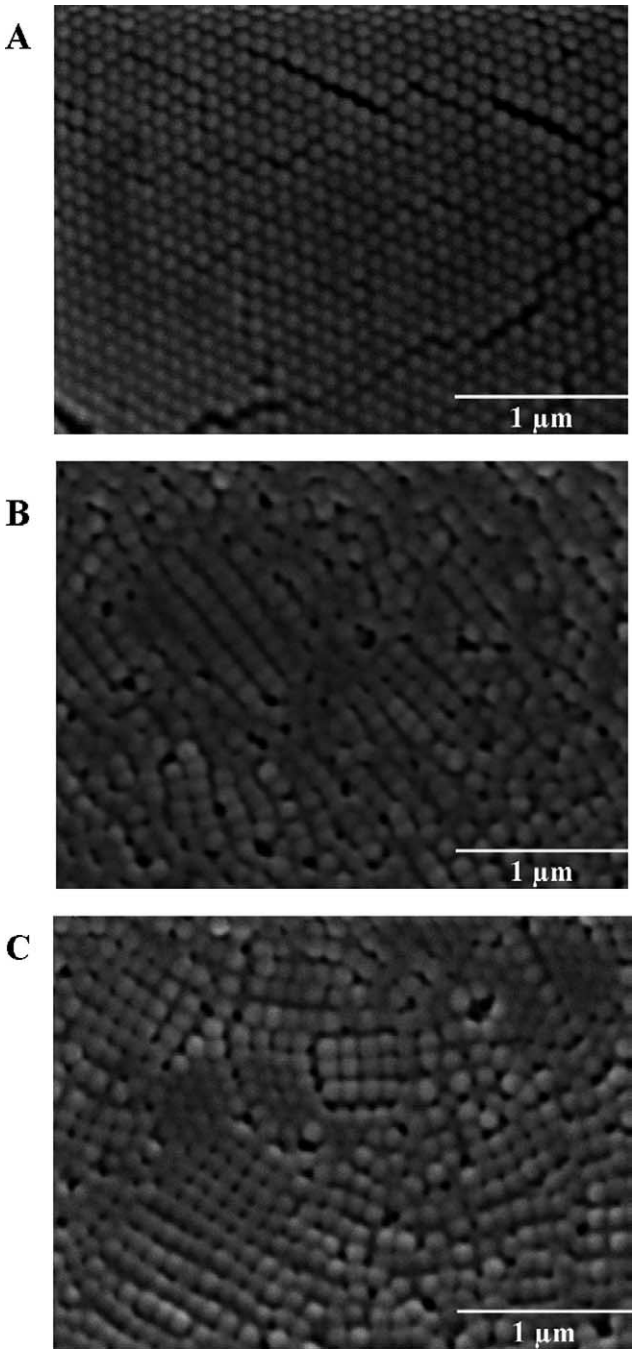

Fig. 1. SEM pictures of the final latex particles: (A) *pmma+10*, (B) *cssgp3* and (C) *cssgpf3*.

than at 25 °C due to the shrinkage of the PNIPAM shell at temperatures higher than the T_{VPT} [16].

The shell thickness increment does not vary in a regular manner with the amount of MBA (see the *cssgp* series in Table 4). Nevertheless, a significant shell ($\delta_{shell}=31$ nm) was obtained for the *cssgp3* latex, which was prepared from a recipe with 1% wt/wt MBA/MMA. Following this, the new latexes were prepared using similar recipes adjusted to include the addition of the functional monomer, AEMH. With the addition of AEMH to the recipe (*cssgpf1–3*), the latexes show a slight increase in diameter at 50 °C but not at 25 °C. Considering that, the PNIPAM chains anchored on the core shrink along the radial directions but not in a direction parallel to the surface [17], the slight increase in the hydrodynamic diameter at 50 °C, probably results from the increase in the intra-electrostatic repulsions during shell shrinkage due to the cationic charges coming from the AEMH co-monomer as its content was raised.

The higher δ_{shell} of *cssgpf4* compared to that of the *cssgpf1* latex, is due to the incorporation of larger amounts of PNIPAM in the shell since its quantity in the recipe was increased by two times (see Table 2).

Fig. 2 shows the variation of the hydrodynamic diameter with temperature for both the *cssgp* (Fig. 2(A)) and the *cssgpf* series (Fig. 2(B)).

Fig. 2(A) shows that above 35 °C, the particle diameter of the *cssgp1–4* latexes is around 150 nm. The *cssgp3* particles show a clear VPT in the temperature range ~20–35 °C, while the *cssgp2* latex does not show any transition and a very diffuse VPT was observed for *cssgp1* and *cssgp4* latexes. This confirms that the 1% wt/wt MBA/MMA ratio used in the *cssgp3* recipe should correspond to the optimal composition at which the desired core-shell morphologies are created.

Fig. 2(B) shows that the VPT of functional core-shell latexes (*cssgpf* series) occurs in a slightly higher temperature range. The transition temperature seems to increase with the amount of AEMH. In fact, for *cssgpf1* and *2* latex particles, the VPT was observed at 30–38 °C while for the *cssgpf3* latex particles it was found to be from 32 to 44 °C. This probably results from the higher electrostatic repulsions due to the protonated amine groups coming from the AEMH co-monomer.

3.3.2. Overall charge density

Table 4 shows the amine and amidine charge densities (σ, μmol/g) coming from the functional monomer (AEMH) and initiator (V50), respectively.

For the *pmma+10* and *cssgp3* latexes, the charge density is only due to the amidine groups. As expected, the *cssgp3* latex exhibits a smaller charge density compared to *pmma+10* because, the added initiator amount was the same and part of the amidine charges were buried during the PNIPAM shell formation. For the *cssgpf1–3* latexes, the surface charge density is higher since besides the amidine charges from the initiator, we have to consider the amine groups coming from the functional monomer. As the functional monomer concentration was raised, a slightly increase in the charge density was observed for the *cssgpf1–3* latex particles. The *cssgpf4* latex has a lower surface charge density than the *cssgpf1* because the shell volume is larger in the first case and the charges are more widely distributed on it.

3.3.3. Electrokinetics

The zeta potential (ζ) of the functional core-shell latexes

Table 4
Particle diameter (D_p), hydrodynamic shell thickness increment (δ_{shell}), swelling factor (SF) and charge density (σ) for *pmma+10* latex, *cssgp1–4* and *cssgpf1–4* core-shell latexes

Latex	$D_P^{25°C}$ (nm)	$D_P^{50°C}$(nm)	δ_{shell} (nm)	SF	σ (μmol/g)
Pmma+10	134	–	–	–	6.9
Cssgp1	165	144	11	1.52	–
Cssgp2	153	148	3	1.12	–
Cssgp3	212	150	31	2.82	3.5
Cssgp4	167	148	10	1.45	–
cssgpf1	203	150	27	2.49	8.6
cssgpf2	223	160	31	2.69	9.0
cssgpf3	210	189	11	1.39	10.8
cssgpf4	245	150	47	4.32	5.9

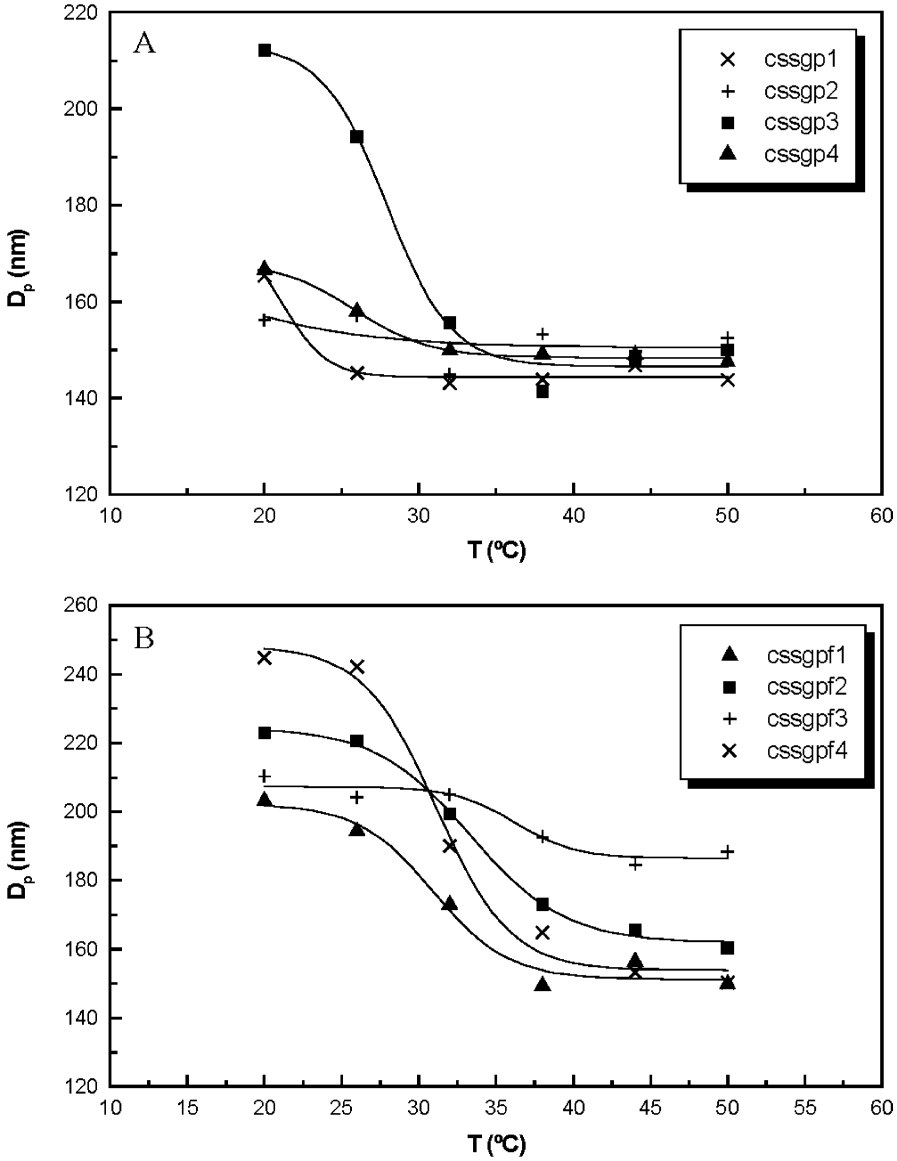

Fig. 2. Variation of the hydrodynamic diameter (D_p) with temperature in 10^{-3} M HCl solutions: (A) *cssgp1* (×), *cssgp2* (+), *cssgp3* (■) and *cssgp4* (▲); (B) *cssgpf1* (▲), *cssgpf2* (■), *cssgpf3* (+) and *cssgpf4* (×).

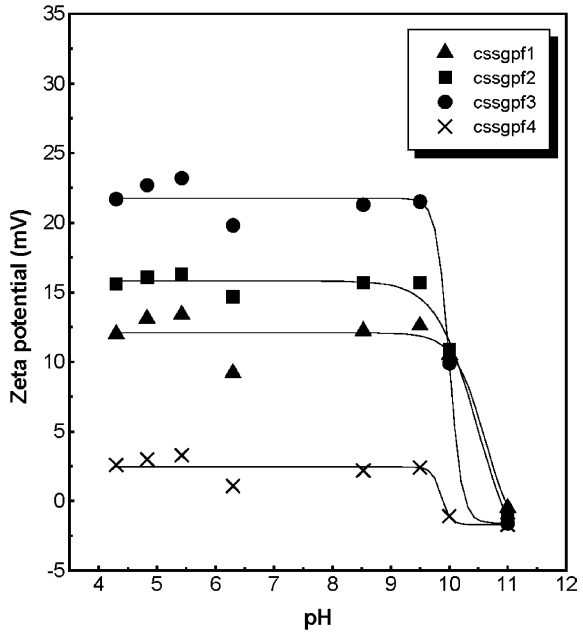

Fig. 3. Variation of the zeta potential (ζ) with pH at 25 °C: *cssgpf1* (▲), *cssgpf2* (■), *cssgpf3* (●) and *cssgpf4* (×).

was determined at 25 °C and several pH values ranging from 4 to 11. Particle surface charge was found to be positive from pH 4 to 9 as shown in Fig. 3 showing that ζ decreases abruptly around pH ~ 9.5, confirming that the isoelectrical point for the latexes coincides with the pKa of the amine and amidine groups [18].

Increasing the AEMH concentration led to a raise in the ζ on the pH range from 4 to 9 (see Fig. 3: *cssgpf1–3*). At this temperature, these latexes have similar particle diameters and the higher ζ obtained only reflects the increase of the surface charge upon AEMH incorporation. The ζ values at 25 °C (pH < 9.5) are higher for the *cssgpf1* than for the *cssgpf4* that has a thicker shell layer. This may be due to differences in the microstructure of the shell layer since the zeta potential depends on the location of the shear plane which is determined by the shell structure (i.e. crosslinking density, charge distribution) [18].

Fig. 4(A) shows the plot of the zeta potential (ζ) as a function of temperature for *pmma + 10* and *cssgp3* latexes.

The ζ values are positive for both latexes as expected since they are positively charged. A value of ζ ~ 36.5 mV, was obtained for the *pmma + 10* latex irrespective of temperature. The ζ values for the *cssgp3* core-shell latex vary from ~ 5 mV at 20 °C to ~ 40 mV at temperatures higher than 40 °C. This variation occurs around the volume phase transition temperature and reflects the shrinkage of the shell during the transition [5]. Above the T_{VPT} the zeta potential of the core-shell particle is, ζ ~ 40 mV, which is identical to that of the pmma + 10 latex. This suggests that above the T_{VPT} all the particles have the same amount of amidine charges distributed in a similar surface.

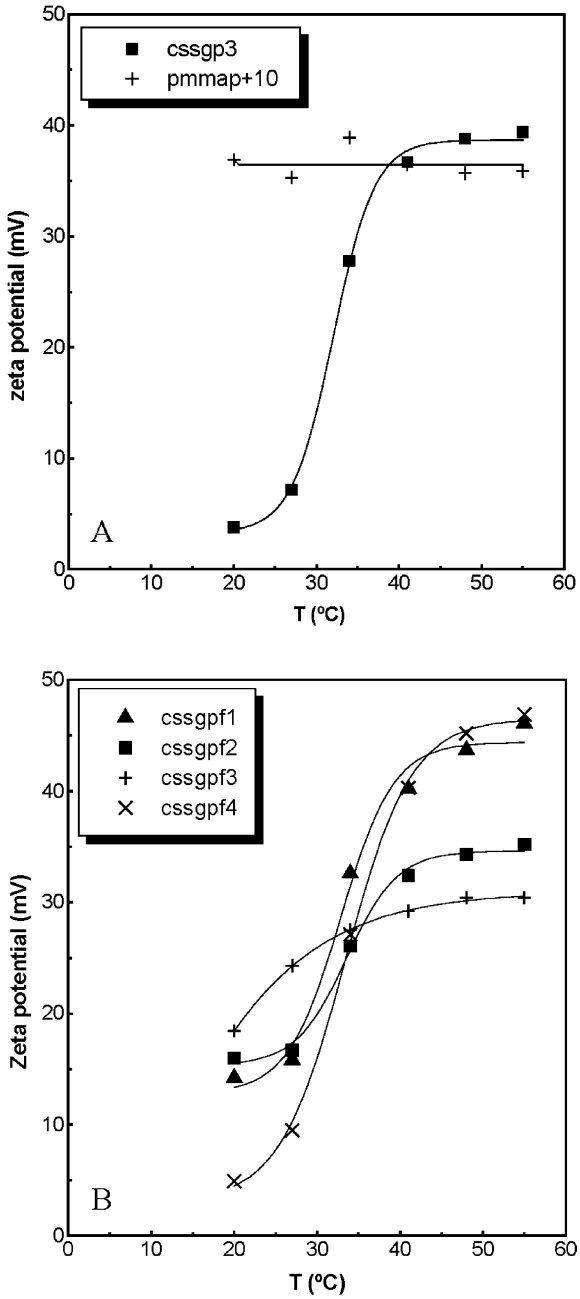

Fig. 4. Variation of the zeta potential (ζ) with temperature for 10^{-3} M HCl solutions: (A) *cssgp3* (■) and *pmmap + 10* (+); (B) *cssgpf1*;(▲), *cssgpf2* (■), *cssgpf3* (+) and *cssgpf4* (×).

Fig. 4(B) shows that the ζ values increase with the amount of AEMH at 20 °C but not at 55 °C. The values at 20 °C are expected since a larger amount of AEMH implies a higher quantity of protonated amide groups in the shell. The fact that this trend was not followed at 55 °C should reflect the differences in shell thickness and charge distribution in the collapsed state.

The zeta potential of *cssgpf1* and *cssgpf4* latexes are identical (~ 46 mV) above the T_{VPT}, despite the difference in the hydrodynamic shell thickness increment of both latexes. This probably results from the fact that above the

T_{VPT} the shell dimensions are negligible and the diameters of both latexes are identical.

4. Conclusions

Thermo-sensitive core-shell PMMA/PNIPAM particles with diameters between 150–250 nm (at 25 °C) and 140–190 nm (at 50 °C) and very low polydispersity were produced by a two-stage emulsion copolymerization process. This was achieved using V50 as initiator and DEDAB as surfactant. The two-stage copolymerization process was found to be more convenient than the batch copolymerization due to the fast reactivity of the monomers and the high water-solubility of MMA. The two-stage polymerization allowed the control of the particle size and size distributions that were determined by the initial MMA/initiator recipe and polymerization conditions in the seed. To increase the surface charge density, the functional monomer AEMH was added in some recipes.

The variation of the particle hydrodynamic diameter with temperature confirms the core-shell morphology of the particles with a PNIPAM shell around the PMMA core. The surface charge density increases with the amount of the co-monomer AEMH, indicating that its incorporation into the shell is efficient. The variation of the zeta potential, ζ, with pH shows that the isoelectric point of the particles is around pH 9.5, which coincides with the pKa of the amine and amidine groups. The variation of the zeta potential with temperature reflects the distribution of charges in the shell volume, which changes around the T_{VPT} due to the thermal sensitivity of the shell.

Acknowledgements

This work was supported by the Fundação para a Ciência e a Tecnoolgia, Portugal, under project POCTI/33866/-QUI/2000 and the Luso-French Scientific and Technical Cooperation Program. A. Santos acknowledges a PhD fellowship from FCT (BD/1227/2000). The authors would like to thank Dr Isabel Nogueira from ICEMS, IST, Portugal for the SEM images.

References

[1] Elaïssari A, editor. Colloidal biomolecules, biomaterials and biomedical applications, vol. 116. New York: Marcel Dekker; 2003.
[2] Hoffman AS. J Controlled Release 1987;6:297–305.
[3] Duracher D, Elaïssari A, Mallet F, Pichot C. Langmuir 2000;16:9002–8.
[4] Kondo A, Kaneko T, Higashitani K. Biotechnol Bioeng 1994;44:1–6.
[5] Pelton R. Adv Colloid Interface Sci 2000;85(1):1–33.
[6] Makino K, Yamamoto S, Fujimoto K, Kawaguchi H, Oshima H. J Colloid Interface Sci 1994;166(1):251–8.
[7] Zhu PW, Napper DH. Phys Rev E 1994;50(2):1360–6.
[8] Duracher D, Sauzedde F, Elaïssari A, Perrin A, Pichot C. Colloid Polym Sci 1998;276(3):219–31.
[9] Xiao XC, Chu LY, Chen WM, Wang S, Li Y. Adv Funct Mater 2003;13(11):847–52.
[10] Smoluchowski V. Bull Akad Sci Bracovie classe Sci Math Natur 1903;1:182.
[11] Delair T, Marguet V, Pichot C, Mandrand B. Colloid Polym Sci 1994;272:962–70.
[12] Santos AM, Elaïssari A, Martinho JMG, Pichot C. Colloid Polym Sci 2003;124:60–3.
[13] Gilbert RG, editor. Emulsion polymerization: a mechanistic approach. London: Academic Press; 1997.
[14] Ferguson CJ, Russell GT, Gilbert RG. Polymer 2002;43:4557–70.
[15] Greenley RZ. In: Brandrup J, Immergut EH, editors. Polymer handbook. New York: Wiley Intersience; 1989. p. 155.
[16] Schild HG. Prog Polym Sci 1992;17(2):163–249.
[17] Dingenouts N, Norhausen C, Ballauff M. Macromolecules 1998;31:8912–7.
[18] Nabzar L, Duracher D, Elaïssari A, Chauveteau G, Pichot C. Langmuir 1998;14(C):5062–9.